SPE 114223

Micromechanics of Hydrate Dissociation in Marine Sediments by Grain-Scale Simulations

Holtzman Ran, SPE, UC Berkeley; **Dmitriy B. Silin**, SPE, UC Berkeley; and **Tad W. Patzek**, SPE, UC Berkeley

This paper was prepared for presentation at the 2008 SPE Western Regional and Pacific Section AAPG Joint Meeting held in Bakersfield, California, U.S.A., 31 March-2 April 2008.

Abstract

We seek to quantify the impact of hydrate dissociation on the strength of hydrate-bearing sediments. Dissociation of gas-hydrates in marine sediments converts the solid hydrate structure into liquid water and gas. Together with the associated pore pressure increase, this process reduces the stiffness of the sediments, which may fracture or be fluidized. If sediment failure occurs, seafloor subsidence and landslides can severely damage offshore infrastructure.

To evaluate the mechanical properties of a sediment sample, we simulate loading of a disordered pack of spherical grains by incremental displacements of its boundaries. The deformation is described as a sequence of equilibrium configurations. Each configuration is characterized by a minimum of the total potential energy. This minimum is computed using a modification of the conjugate gradient algorithm. We verify our model against published data from experiments on glass beads. Our simulations capture the nonlinear, path-dependent behavior of granular materials observed in experiments.

Hydrates are modeled as load-bearing solid particles within the pores. To simulate the consequences of dissociation, we reduce the solid fraction by shrinking the hydrate grains. The effect of the associated excess pore pressure is modeled by isotropic compression of the solid grains, and reduction in macroscopic effective stress. Weakening of the sediment is quantified as a reduction of the effective elastic moduli.

Introduction

Gas-hydrates are solid materials formed under a range of high pressures and low temperatures. Dissociation converts them into liquid water and free gas. The volumetric expansion of gas can lead to an appreciable increase in pore pressure,[1] reducing the effective stress. Thus, dissociation impacts the mechanical properties of hydrate-bearing sediments (HBS) by reducing both the solid fraction and the effective stress. Hydrate dissociation caused, for instance, by hot fluids produced from deep formations, can destabilize the ocean floor and lead to massive landslides[1] that can damage nearby structures such as off-shore platforms.

On the one hand, obtaining undisturbed HBS samples requires special coring which preserves the in-situ conditions. On the other hand, artificial creation of representative samples is difficult.[2] For these reasons, there is no single definitive model for the distribution of hydrates within the pore space.[3] This distribution depends on the formation mechanism, along with many other factors.

We seek to evaluate the mechanical response to dissociation of gas-hydrates in marine sediments. The response of composite materials such as HBS is determined by the interactions among discrete grains. Grain-scale numerical simulations have become a valuable tool in the study of granular materials.[4,5] Most grain-scale simulations are based on the Discrete Element Method (DEM).[6] In DEM, interactions between the particles are treated as a dynamic process, accounting for the inertia of the grains. However, tight constraints imposed on the time step used in the numerical integration,[7] make DEM simulations time-consuming. To accelerate computations and damp grain oscillations, material properties such as the density of the

grains and their contact stiffness are often adjusted[8,9] to unrealistic values.

In this paper, a physically-based discrete model is presented. We simulate an irregular pack of spherical grains, loaded by incremental displacements of its boundaries. The contact forces are determined by the Hertzian model, assuming frictionless contacts. Using a quasi-static model, we find the equilibrium configurations using a modification of the conjugate gradient (CG)[10] algorithm. This efficient computational procedure, implemented in Matlab by Holtzman, is also utilized to generate a dense initial arrangement required for simulations. The interactions between the hydrate and the sediment are considered from both the grain and the sample scale. The degradation of sediment strength is quantified via the reduction in elastic moduli.

Simulating quasi-static deformation

We simulate an experiment on a sample made of cohesionless grains in a rectangular container. The sample is loaded by incremental displacements of the container walls, allowing the grains to reach static equilibrium following each perturbation. Each equilibrium configuration is computed by minimizing the total potential energy of the system. The initial conditions are the positions of the grains, prior to the simulated test. The positions and orientations of the container walls provide for the boundary conditions.

Grain pack model. We model granular materials as a three-dimensional (3D) irregular ("random") packing of spherical grains, see **Fig. 1**. The grains are assumed to be homogenous and isotropic. To model heterogenous materials such as clastic sediments, we assign the grain properties from a given distribution of sizes and elastic moduli. The deformations are assumed to be small and localized near the contacts, allowing to approximate the shape of a deformed grain by a sphere. We hypothesize here that in a tight packing, the macroscopic stress is mostly affected by the normal component of the contact forces.[8,11,12] This assumption is based on the argument that the size of the asperities that resist lateral or angular displacements is much smaller than the size of the grains themselves. Thus, we only account for the normal force components.

The orientation and rotations of the grains are of no importance under the assumption of frictionless contact between spherical grains. In a fixed coordinate system, each grain is fully described by the coordinates of its center and its radius. Each configuration is characterized by the positions of the grain centers, providing $3N$ degrees of freedom for a pack of N grains. Given a reference configuration in equilibrium, we perturb the boundary conditions, forcing the grains to deform and rearrange to a new equilibrium configuration ("current"). Labeling all grains with a single index $i = 1, 2, \ldots, N$, we denote the radius-vector of the center of grain i by $\boldsymbol{r}_i$. Let $\boldsymbol{u}_i$ denote the displacement of grain i: $\boldsymbol{u}_i = \boldsymbol{r}_i - \boldsymbol{r}_{i(0)}$, where subscript (0) denotes the reference configuration, see Fig. 1. The radius of body i is

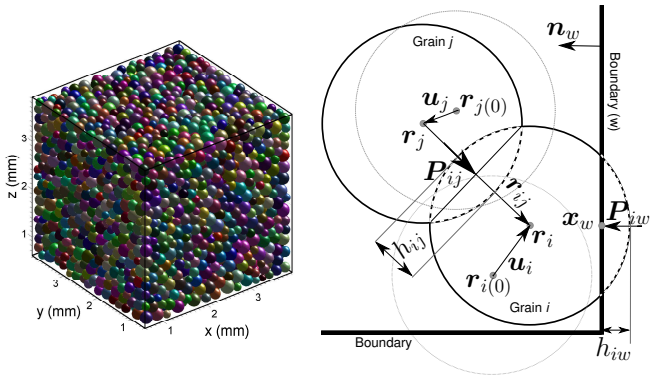

Fig. 1: Left: a typical pack with 5036 grains used in the numerical simulations. Right: schematic description of the contact geometry. The initial configuration of the grains is marked with grey dotted lines. The dashed lines represent grain overlap caused by deformations.

R_i, its mass is m_i, and the Young's modulus and Poisson's ratio of its material are E_i and ν_i, respectively. Subscript w denotes a boundary wall, $w = 1, 2, \ldots, 6$.

Contact model. According to Hertzian contact theory, the magnitude of the compressive normal force acting at the contact between a pair of grains i and j is

$$\|\boldsymbol{P}_{ij}\| = \frac{4}{3} E^*_{ij} \left(R^*_{ij}\right)^{1/2} \left(h_{ij}\right)^{3/2} \tag{1}$$

where $\|\boldsymbol{a}\| = (\boldsymbol{a} \cdot \boldsymbol{a})^{1/2}$ is the magnitude of a vector $\boldsymbol{a}$. Parameters $R^*_{ij} = \left(\frac{1}{R_i} + \frac{1}{R_j}\right)^{-1}$ and $E^* = \left[\frac{(1-\nu_i^2)}{E_i} + \frac{(1-\nu_j^2)}{E_j}\right]^{-1}$ are the effective radius and elastic coefficient associated with that contact, respectively. Eq. (1) is applicable to a grain-boundary contact, by modeling the latter as a grain of an infinite radius. The contact deformation is measured by the overlap $h_{ij} \geq 0$,

$$\begin{aligned} h_{ij} &= R_i + R_j - \|\boldsymbol{r}_{ij}\| && \text{for grain-grain contact} \\ h_{iw} &= R_i - (\boldsymbol{r}_i - \boldsymbol{x}_w) \cdot \boldsymbol{n}_w && \text{for grain-boundary contact} \end{aligned} \tag{2}$$

where $\boldsymbol{r}_{ij} = \boldsymbol{r}_i - \boldsymbol{r}_j$, $\boldsymbol{x}_w$ denotes the initial contact point with the wall w, and $\boldsymbol{n}_w$ is an inward unit normal to the wall, see Fig. 1. Here the orientation $\boldsymbol{n}_w$ was held fixed, and thus $\boldsymbol{x}_w$ can be chosen arbitrarily on w. The force acting on grain i at the contact with another grain j or a wall w is directed along $\boldsymbol{r}_{ij}$ or $\boldsymbol{n}_w$, respectively. Thus, no moment relative to the center of the grain is developed.

Obtaining equilibrium configurations. At equilibrium, the balance of forces for each grain yields three scalar equations. For N grains, the total number of equations is $3N$. The unknowns, i.e. the grain displacements, can be

written as a column vector $\boldsymbol{\theta} = [\boldsymbol{u}_1 \dots \boldsymbol{u}_N]^T$, where $\boldsymbol{u}_i$ is a row vector, and superscript T is the transpose. The exponent of 3/2 in Eq. (1) makes the system of equations nonlinear.

We seek an equilibrium configuration by employing an equivalent variational formulation. Namely, an equilibrium configuration is characterized by a set of displacements $\boldsymbol{\theta}$ corresponding to a minimum of the total potential energy of the system. This energy is a function of the deformations (strain energy) and the gravitational energy of the grains. The elastic strain energy of a pair of bodies in contact is equal to the sum of work done on each body to deform it. This work is the dot product of the force with the displacement increment, integrated over the total displacement. Thus, the strain energy U_{ij} stored in the deformed contact region between bodies i and j is (cf. Eq. (9.15) in Ref.[13])

$$U_{ij}(\boldsymbol{u}_i, \boldsymbol{u}_j) = \frac{8E^*_{ij}(R^*_{ij})^{1/2}}{15}(h_{ij})^{5/2} \tag{3}$$

The total potential energy of the system is the sum of the strain energy of all contacts and the gravitational potentials of all grains

$$\Pi(\boldsymbol{\theta}) = \sum_{i=1}^{N} \left\{ \frac{1}{2}\sum_{j=1}^{N^i_g} U_{ij} + \sum_{w=1}^{N^i_b} U_{iw} + m_i g(\boldsymbol{r}_i \cdot \hat{\boldsymbol{e}}_z - z^*) \right\} \tag{4}$$

Here z^* is an arbitrary fixed reference elevation, $\hat{\boldsymbol{e}}_z$ is a unit vector pointing opposite to the direction of gravity, and g is the gravity acceleration. N^i_g and N^i_b are the number of contacts for grain i with other grains and boundaries, respectively. Their sum $N^i_g + N^i_b$ is the coordination number of that grain. Note that the set of contacts for each grain varies with the deformation of the pack, introducing additional nonlinearity.

The gradient of Π with respect to $\boldsymbol{\theta}$ is a column vector $\nabla_{\boldsymbol{\theta}}\Pi = -[\boldsymbol{F}_1 \dots \boldsymbol{F}_N]^T$, where the row vector $\boldsymbol{F}_i$ is the sum of forces on grain i,

$$\boldsymbol{F}_i = \sum_{j=1}^{N^i_g} \boldsymbol{P}_{ij} + \sum_{w=1}^{N^i_b} \boldsymbol{P}_{iw} - m_i g \hat{\boldsymbol{e}}_z \tag{5}$$

Thus, the vanishing gradient of Π is equivalent to the balance of forces. This minimum is found numerically using a modification of the CG algorithm, see Appendix.

Initial grain pack generation. Simulations of a deforming grain pack requires a sufficiently dense initial configuration.[14,15] Such an initial configuration could be obtained from a physical sample, e.g. using MRI[16] or X-ray tomography imaging.[17] However, these techniques are cumbersome. Alternatively, an initial irregular configuration could be generated numerically using wither "constructive" or "dynamic" algorithms. Constructive algorithms are based on geometry alone and thus require relatively small computing time; however, the current state-of-the-art constructive algorithms produce 3D arrangements with low coordination numbers, gaps, or anisotropic structure.[15] In dynamic algorithms, a loose packing is created by placing a relatively small number of grains in a bounded domain. Then, its density is increased by either expanding the grains or moving the boundaries closer together. A static equilibrium configuration is found by simulating intergranular interactions, e.g. using DEM. The large number of collisions and grain rearrangements makes such a procedure very time-consuming.[15]

Instead, we use our quasi-static algorithm, which provides an efficient alternative to DEM. Here, we start by selecting a portion of a pack generated by DEM,[18] bounding it by a rectangular domain. This packing is loose, with many grains supported by less than 4 contacts, rendering them mechanically unstable. To obtain a denser packing we first expand these unstable grains, until their coordination number reaches 4. Then, we shrink the pack by equal displacements of all boundaries, and apply our algorithm to obtain an equilibrium configuration. This process is repeated until practically* all grains have coordination number of 4 or more, and appreciable contact forces develop.

Evaluating macroscopic stress and strain. Macroscopic, continuum parameters such as stress and strain can be obtained from grain-scale parameters by spatial averaging. However, there are several methods for transforming between discrete and continuum parameters, in particular for the strain.[19] Here we consider the pack to be a homogenous representative volume of a larger medium, and compute the average stress and strain within this volume as described below.

The external normal forces applied on the boundaries are calculated from the sum of the contact forces on the container walls. The average normal stresses are evaluated by dividing these external forces by the area of the respective walls. To confirm the validity of our stress evaluation procedure, we also calculate the averaged Cauchy stress, taking into account the entire set of contact forces within the sample volume.[20] This calculation yielded similar values to those obtained from our procedure.

To estimate numerically the macroscopic strains $\boldsymbol{\epsilon} = \frac{1}{2}\left[\nabla_{\boldsymbol{x}}\boldsymbol{u} + (\nabla_{\boldsymbol{x}}\boldsymbol{u})^T\right]/2$, we replace the derivatives with finite differences. In the last equation $\boldsymbol{x}$ is a radius-vector to an infinitesimal volume, and $\boldsymbol{u}$ is its displacement.[13] For a rectangular domain, the normal strain in the l-direction ($l = 1, 2, 3$) reduces to $\Delta L_l / L_{l(0)}$, where $\Delta L_l = L_l - L_{l(0)}$, L_l and $L_{l(0)}$ being the current and the reference (undeformed) length of the domain in that direction, respectively. In our simulations, the macroscopic strains serve as boundary conditions, enforced by displacing the container walls. By applying uniform or different normal strains in three principal directions, we simulate an isotopic or

*A complete elimination of unstable grains may not be possible[11] because of grain sizes variation: the opening between large grains can be large enough to contain a small grain, not in stable equilibrium.

a polyaxial test. A uniaxial test is simulated by applying strain in a single direction.

Macroscopic elastic moduli. To describe mechanical properties as they evolve with the deformation, we discretize the load path and assign a set of constant effective elastic moduli for each loading interval. The moduli for each interval are evaluated by fitting the stress-strain results with Hooke's law. Hooke's law for a homogenous, isotropic body is $\boldsymbol{\sigma} = \lambda \mathrm{tr}(\boldsymbol{\epsilon})\hat{\boldsymbol{I}} + 2G\boldsymbol{\epsilon}$, where $\boldsymbol{\sigma}$ is the stress tensor, $\mathrm{tr}(\boldsymbol{\epsilon})$ is the trace of $\boldsymbol{\epsilon}$, and $\hat{\boldsymbol{I}}$ is the unit second order tensor. The moduli λ and G are Lame's constant and the shear modulus, respectively. Other elastic moduli can be evaluated from λ and G.[13]

The moduli evaluated using the procedure above are the bulk-averaged, effective moduli, corresponding to an effective homogeneous and isotropic elastic medium. Because the moduli depend on the deformation, stress-induced anisotropy can develop when loads in different directions are significantly different,[21] as observed in our simulations. To verify whether a grain pack is isotropic, we simulate a polyaxial test and compare the moduli for each pair of principal directions. If they are similar within a given tolerance, we consider the response isotropic. We minimized stress-induced anisotropy by applying relatively isotropic strains, evaluating the moduli at different loads by a uniaxial test. Anisotropy can also develop if the number of grains in the pack is too small, as macroscopically isotropic systems may exhibit local anisotropy.[22] To avoid such scale-related anisotropy, we used packs with sides not smaller than ∼15 grain diameters. This length scale depends on the properties of the grains and their spatial arrangement, and was determined by trial and error. As a result of using the above measures, the estimates of the moduli in different directions were practically identical.

Model verification

Input parameters. To verify our model, we compare our estimated macroscopic moduli with those measured in experiments on spherical and relatively smooth glass beads. The elastic moduli of the grains were assigned mean values of $\bar{E} = 70$ GPa for Young's modulus and $\bar{\nu} = 0.2$ for Poisson's ratios.[23] In other simulations, quartz sand was modeled by assigning $\bar{E} = 100$ GPa and $\bar{\nu} = 0.15$.[24,25] The elastic moduli were normally distributed with a standard deviation of 10% of the mean. The radii of the grains were distributed uniformly between 0.07-0.13 mm. The density of both types of grains was taken to be 2.65 g/cm^3, Ref.[24]

Stress-Strain. To capture hysteresis and stress-induced anisotropy, we simulated loading-unloading cycle in a polyaxial test, on a pack of 2654 quartz grains (denoted by QUARTZ2654). The porosity and mean coordination number varied as 35.8-30.8% and 7.23-8.26, accordingly, with stresses of ∼50-300 MPa. To verify our model against experiments on glass beads, we simulated a test on a pack of 5036 glass beads (GLASS5036). For

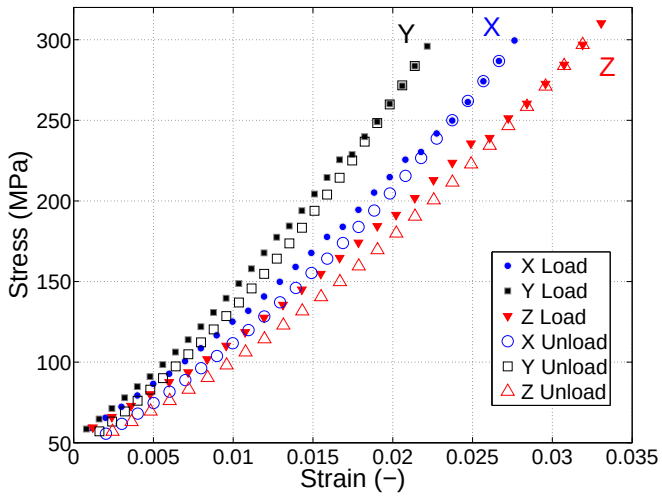

Fig. 2: Stress-strain curves obtained from numerical simulations of loading and unloading in a polyaxial test on QUARTZ2654. Hysteresis is evident as different loading and unloading curves.

GLASS5036, the porosity and mean coordination number varied as 37.1-35.7% and 6.48-6.97, accordingly, with stresses of ∼1-22 MPa. The stress-strain curves calculated for QUARTZ2654 are plotted in **Fig. 2**. A stress drop is noticeable, associated with variations in the complex network of contacts ("fabric") and contact forces.[5] Some of these microstructural variations are irreversible, contributing to the hysteretic response observed in experiments.[26] This hysteresis is evident in Fig. 2 as different loading and unloading curves. A more elaborate discussion and additional results will be published elsewhere.

Elastic moduli. The macroscopic elastic moduli for different stages of isotropic compression were evaluated for sample GLASS5036 by a uniaxial test. These moduli estimates are plotted in **Fig. 3** vs. the confining stress σ_c, defined by the mean of the lateral stresses perpendicular to the principal loading direction. The bulk modulus K estimates are in agreement with calculations from acoustic velocity data measured in experiments on glass beads,[23,27,28] though some values are slightly lower than the data. In addition, our predicted rate of moduli growth with σ_c agrees with the data, indicating that the moduli grow faster than the power law ${\sigma_c}^{1/3}$ predicted by the effective medium theory (EMT).[23]

At the same time, our shear modulus strongly underestimates the experimental data. In particular, at lower stresses, the evaluated shear modulus drops sharply, becoming negligibly small as the mean coordination number approaches 6 and the porosity exceeds ∼37%. Similar loss of shear rigidity was observed in DEM simulations using a frictionless contact model.[29] We consider the discrepancies between our predictions and the data to be caused by the frictionless contact assumption, as the shear modulus greatly depends on the intergranular shear.[29]

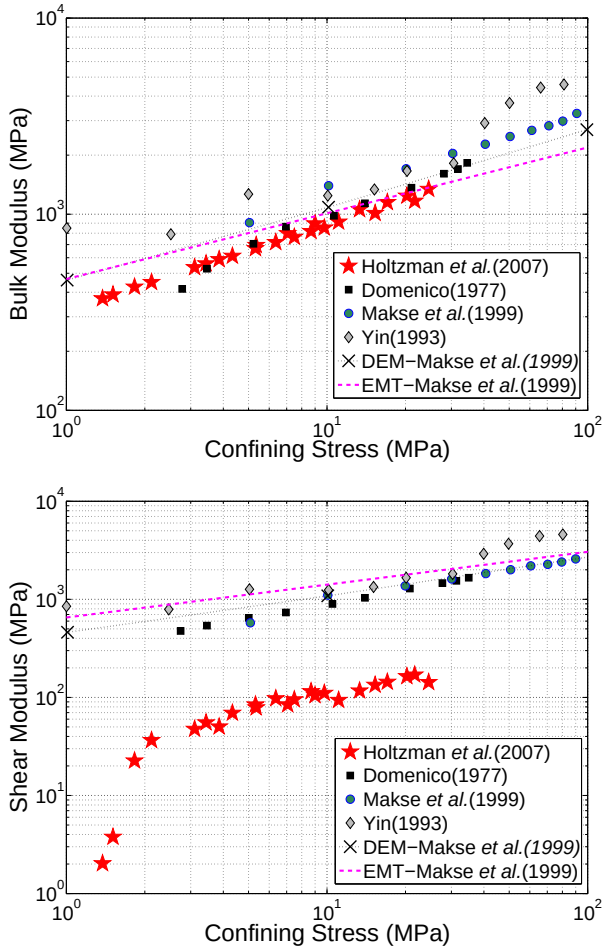

Fig. 3: The evaluated effective bulk (top) and shear (bottom) modulus from our simulations using GLASS5036 vs. the confining stress σ_c. Also shown are calculations from acoustic velocities measured in glass beads,[23,27,28] in addition to results from DEM simulations and effective medium theory (EMT),[23] obtained by digitizing Figure 1 in Ref.[23]

Impact of hydrate dissociation

Modeling hydrate dissociation. We use the procedure described above to quantify the mechanical response to hydrate dissociation in HBS. Dissociation impacts the mechanical properties of HBS by reducing both the solid fraction and the effective stress. The excess pressure due to dissociation varies with factors such as dissociation rate, sediment permeability, and initial pore pressure.[1] Predicting this excess pressure as a function of dissociation is outside the scope of this paper. Thus, we consider a number of dissociation scenarios, for a range of possible dissociation amounts and excess pressures. This range, taken from other models,[1] is used as input parameters in our simulations.

To model the interaction between the sediment and the hydrate, we consider methane-hydrate formed preferentially in the larger pores, rather than in the pore-throats. Such distribution makes hydrates a part of the granular frame, i.e. load-bearing solid particles. Such hydrate distribution can represent sediments with low hydrate saturation, where the gas is slowly introduced in the aqueous phase.[2] The distribution of hydrates within the pore space depends on the formation mechanism, among other factors, and a wide variety of distribution models exists.[3]

The hydrate saturation is defined by $S = V^h/V$, where V^h is the volume occupied by hydrate and V is the total pore volume (including the hydrate). We quantify the amount of dissociation by the decrement of hydrate saturation $\Delta S < 0$, decreasing the saturation to $S + \Delta S$. The reduction in solid fraction due to dissociation is modeled by shrinking the hydrate grains. The impact of the excess pore pressure p_{ex} is modeled at both the grain and the sample level. At the grain scale, with the assumption of small deformations, the contact area is much smaller than the surface area of the grains. Thus, assuming uniform pore pressure within the sample, the grains experience isotropic compression, with a net force applied by the fluid pressure which is practically zero. The volume of grain i, V_i, changes by $\Delta V_i < 0$, determined by $-p_{ex} = K_i \epsilon_{kk,i}$, where K_i and $\epsilon_{kk,i}$ are the bulk modulus and the volumetric strain of grain i, respectively. For small changes, $\epsilon_{kk,i} \approx \Delta V_i/V_i$. At the sample scale, the reduction in effective stress is modeled by applying a tensile macroscopic strain $\epsilon_{kk} > 0$, expanding the sample isotropically. This strain is determined from the poroelastic constitutive equation $\alpha_{bw} p_{ex} = K \epsilon_{kk}$, where α_{bw} is the Biot-Willis coefficient.[30]

Elastic moduli reduction by hydrate dissociation. The effect of dissociation in HBS is quantified via the evolution of the elastic moduli. The initial state of an HBS sample is modeled as a dense arrangement of spherical grains, where some of the smallest grains are considered to be methane-hydrate. These hydrate grains are linearly-elastic, with moduli of $E = 6.6$ GPa and $\nu = 0.32$ and density of 0.9 g/cm^3, Ref.[31] To model quartz sand as the host sediment, the other grains were assigned properties of quartz. The initial porosity and hydrate saturation was $\phi \approx 45\%$ and $S = 0.215$, respectively. The effective stress for this initial packing, determined from the contact forces on the walls, was $\sim$21 MPa. The pack is considered to be under a specified initial pore pressure, which may be larger than hydrostatic pressure if the sediment is confined by a low-permeability layer. The resulting total stress, which is considered fixed in our simulations, can exceed the lithostatic stress if the sediment carries the weight of a nearby off-shore platform.

By varying the excess pressure p_{ex} and the saturation reduction ΔS independently, we produce a series of configurations, covering a range of possible scenarios. For each configuration, the elastic moduli are evaluated by simulating a uniaxial test. In **Fig. 4** (top), these moduli are plotted against the excess pressure p_{ex}, for a fixed change in saturation $\Delta S = -0.01$. Conversely, Fig. 4 (bottom) shows the moduli as functions of ΔS, for a fixed pressure $p_{ex} = 1$ MPa. The initial moduli prior to dissociation are

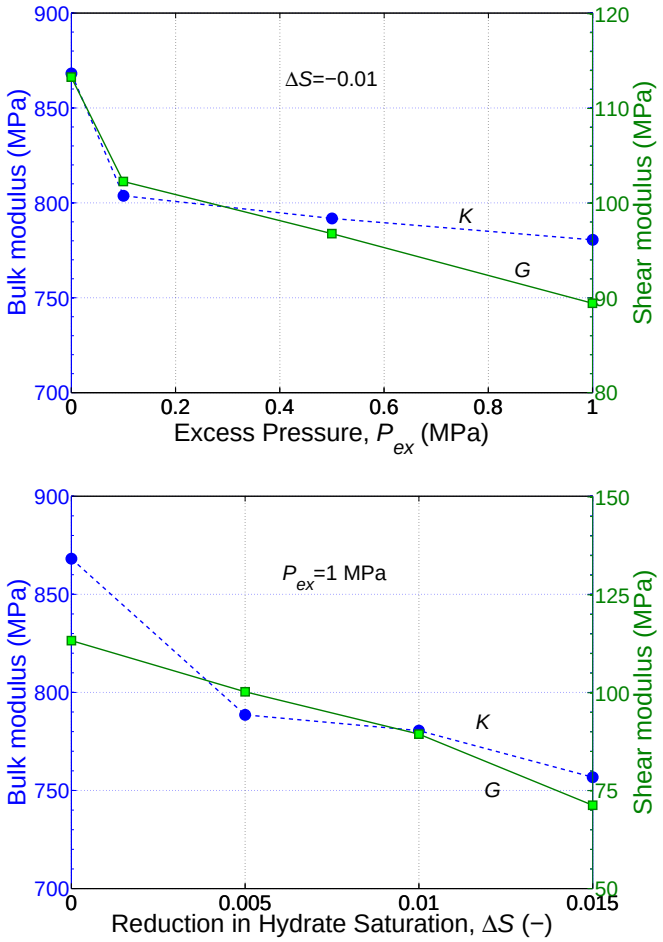

Fig. 4: Simulating reduction in bulk (dashed line) and shear (solid) modulus due to hydrate dissociation. Top: varying the excess pore pressure p_{ex}, for a fixed saturation decrement $\Delta S = -0.01$. Bottom: varying the saturation decrement ΔS, for a fixed excess pressures $p_{ex} = 1$ MPa.

plotted in the left-most parts of both figures. We used a value of $\alpha_{bw} = 0.8$, corresponding to that of sand.[25]

Weakening of HBS is evident from a reduction in elastic moduli, as the sediment becomes looser and softer. This observation is in qualitative agreement with experiments[2,3] and other numerical simulations.[32] Further dissociation may lead to a significant decrease in the solid support, reaching a critical state with loss of shear rigidity. In such a state, the sediment is more susceptible to landslides and subsidence, threatening the safety of adjacent off-shore platforms.

Discussion and conclusions

We quantify the mechanical effect of hydrate dissociation in marine sediments using grain-scale simulations. We describe HBS as a granular material, modeling an HBS sample as a three-dimensional, disordered packing of elastic spherical grains, bounded by a rectangular container.

We use a quasi-static model, where the pack is loaded by incremental displacements of the container walls. Each equilibrium configuration is found by minimizing the total potential energy of the system. A modification of the conjugate gradient algorithm is used to obtain this minimum. This approach results in an efficient computational procedure, which is also used to generate a dense initial arrangement.

The macroscopic stress, strain, and elastic moduli are evaluated from the contact forces and the displacements of the boundaries. Our results capture the nonlinear and path-dependent macroscopic strain-stress response observed in experiments, such as loading and unloading hysteresis.

We have verified our physics-based model against available experimental data. The good agreement between predicted and measured values of the macroscopic bulk modulus has been achieved with no adjustments of the relevant material properties. The macroscopic shear modulus evaluated from the simulations underestimates typical experimental data. We attribute this deficiency to the frictionless contact model employed, using the Hertzian contact theory. A more advanced model accounting for friction and inter-granular cementation will be presented elsewhere.

Hydrates are modeled as load-bearing solid particles within the pores. To simulate the consequences of dissociation, we reduce the solid fraction by shrinking the hydrate grains. The effect of the associated excess pore pressure is modeled by isotropic compression of the solid grains, and reduction in macroscopic effective stress.

A series of possible scenarios has been simulated, showing degradation of sediment strength as a reduction in the macroscopic elastic moduli. This trend agrees qualitatively with the published results of experiments and numerical simulations. Further dissociation might lead to a loss of solid support of the skeleton, causing seafloor instabilities such as landslides and subsidence. To predict such instabilities and their possible impact on off-shore platforms, our model can be used to produce constitutive relationships for large-scale simulations (e.g. Ref.[32]).

Acknowledgements

This work was supported by the Assistant Secretary for Fossil Energy, Office of Natural Gas and Petroleum Technology, through the National Energy Technology Laboratory, under the U.S. Department of Energy, Contract #DE-FC26-05NT42664.

References

[1] W. Xu and L. N. Germanovich. Excess pore pressure resulting from methane hydrate dissociation in marine sediments: A theoretical approach. *Journal of Geophysical Research*, 111:B01104, 2006.

[2] T. S. Yun, J. C. Santamarina, and C. Ruppel. Mechanical properties of sand, silt, and clay containing tetrahydrofuran hydrate. *Journal of Geophysical Research*, 112(B04106), 2007.

[3] W. Durham, L. Stern, S. Kirby, and S. Circone. Rheological comparisons and structural imaging of sI and

sII endmember gas hydrates and hydrate/sediment aggregates. In *Proceedings of the 5th International Conference on Gas Hydrates, 26-29 September 2004*, Trondheim, Norway, 2005.

[4] H. Kruggel-Emden, E. Simsek, S. Rickelt, S. Wirtz, and V. Scherer. Review and extension of normal force models for the discrete element method. *Powder Technology*, 171(3):157–173, 2007.

[5] A. A. Peña, A. Lizcano, F. Alonso-Marroquin, and H. J. Herrmann. Biaxial test simulations using a packing of polygonal particles. *International Journal for Numerical and Analytical Methods in Geomechanics*, 32(2):143–160, 2008.

[6] P. A. Cundall and O. D. L. Strack. A discrete numerical model for granular assemblies. *Geotechnique*, 29:47–65, 1979.

[7] C. O'Sullivan and J. D. Bray. Selecting a suitable time-step for discrete element simulations that use the central difference time integration approach. *Engineering Computations*, 21(2–4):278–303, 2004.

[8] C. Thornton. Numerical simulations of deviatoric shear deformation of granular media. *Geotechnique*, 50(1):43–53, 2000.

[9] C. O'Sullivan, J. D. Bray, and M. Riemer. Examination of the response of regularly packed specimens of spherical particles using physical tests and discrete element simulations. *Journal of Engineering Mechanics*, 130(10):1140–1150, 2004.

[10] W. H. Press, B. P. Flannery, S. A. Teukolsky, and W. T. Vetterling. *Numerical Recipes in Fortran 77*. Cambridge University Press, New York, 1986.

[11] C. Thornton and S. J. Antony. Quasi-static deformation of particulate media. *Philosophical Transactions of the Royal Society A: Mathematical, Physical and Engineering Sciences*, 356(1747):2763–2782, 1998.

[12] L. Rothenburg and R. J. Bathurst. Analytical study of induced anisotropy in idealized granular-materials. *Geotechnique*, 39(4):601–614, 1989.

[13] L. D. Landau and E. M. Lifshitz. *Theory of Elasticity*. Course of Theoretical Physics, Vol 7. Elsevier, Burlington, MA, 1986.

[14] C. O'Sullivan. *The application of discrete element modelling to finite deformation problems in geomechanics*. PhD thesis, University of California, Berkeley, CA, 2002.

[15] K. Bagi. An algorithm to generate random dense arrangements for discrete element simulations of granular assemblies. *Granular Matter*, 7(1):31–43, 2005.

[16] T. T. Ng and C. Wang. Comparison of a 3-D DEM simulation with MRI data. *International Journal for Numerical and Analytical Methods in Geomechanics*, 25(5):497–507, 2001.

[17] Yanrong Fu. *Experimental Quantification and DEM Simulation of Micro-Macro Behaviors of Granular Materials Using X-ray Tomography Imaging*. PhD thesis, University of Louisiana, Baton Rouge, LA, 2005.

[18] G. Jin. *Physics-Based Modeling of Sedimentary Rock Formation and Prediction of Transport Properties*. PhD thesis, University of California, Berkeley, CA, 2006.

[19] K. Bagi. Analysis of microstructural strain tensors for granular assemblies. *International Journal of Solids and Structures*, 43(10):3166–3184, 2006.

[20] J. Christoffersen, M. M. Mehrabadi, and S. Nemat-Nasser. A micromechanical description of granular material behavior. *Journal of Applied Mechanics*, 48(2):339–344, 1981.

[21] D. L. Johnson, L. M. Schwartz, D. Elata, J. G. Berryman, B. Hornby, and A. N. Norris. Linear and nonlinear elasticity of granular media: stress-induced anisotropy of a random sphere pack. *Journal of Applied Mechanics*, 65:380–388, 1998.

[22] I. Goldenhirsch and C. Goldenberg. Stress in dense granular materials. In H. Hinrichsen and D. E. Wolf, editors, *The Physics of Granular Media*. Wiley-VCH, 2005.

[23] H. A. Makse, N. Gland, D. L. Johnson, and L. M. Schwartz. Why effective medium theory fails in granular materials. *Physical Review Letters*, 83(24):5070–5073, 1999.

[24] R. N. Yong. *Soil properties and behaviour*. Developments in geotechnical engineering. Elsevier Scientific Pub. Co., Amsterdam; New York, 1975.

[25] D. J. Hart and H. F. Wang. Laboratory measurements of a complete set of poroelastic moduli for Berea sandstone and Indian limestone. *Journal of Geophysical Research*, 100(B9):17741–17751, 1995.

[26] Jyh-Chau Liou and Yii-Wen Pan. Fabric evolution of granular assembly under *K0* loading/unloading. *International Journal for Numerical and Analytical Methods in Geomechanics*, 27(13):1099–1122, 2003.

[27] S. N. Domenico. Elastic properties of unconsolidated porous sand reservoirs. *Geophysics*, 42(7):1339–1368, 1977.

[28] Hezhu Yin. *Acoustic velocity and attenuation of rocks: isotropy, intrinsic anisotropy, and stress-induced anisotropy*. PhD thesis, Stanford University, Stanford, CA, 1993.

[29] Hernan A. Makse, Nicolas Gland, David L. Johnson, and Lawrence Schwartz. Granular packings: nonlinear elasticity, sound propagation and collective relaxation dynamics. *Physical Review E*, 70:061302, 2004.

[30] M. A. Biot and D. G. Willis. The elastic coefficients of the theory of consolidation. *Journal of Applied Mechanics*, 24:594–601, 1957.

[31] Gilles Guerin. *Acoustic and Thermal Characterization of Oil Migration, Gas Hydrates Formation and Silica Diagenesis*. PhD thesis, Columbia University, New York, NY, 2000.

[32] Jonny Rutqvist and George J. Moridis. Numerical studies of geomechanical stability of hydrate-bearing sediments. In *2007 Offshore Technology Conference, 30 April - 3 May*, Houston, TX, 2007.